



## Electrochemical performances of $Mg_{45}M_5Co_{50}$ (M=Pd, Zr) ternary hydrogen storage electrodes

Le-yu ZHAN<sup>1</sup>, Yao ZHANG<sup>1</sup>, Yun-feng ZHU<sup>2</sup>, Xiang-yang ZHUANG<sup>1</sup>, Neng WAN<sup>3</sup>,  
Yi QU<sup>4</sup>, Xin-li GUO<sup>1</sup>, Jian CHEN<sup>1</sup>, Zeng-mei WANG<sup>1</sup>, Li-quan LI<sup>2</sup>

1. School of Materials Science and Engineering, Southeast University, Nanjing 211189, China;

2. College of Materials Science and Engineering, Nanjing Tech University, Nanjing 210009, China;

3. School of Electronics Science and Engineering, Southeast University, Nanjing 210096, China;

4. Dalian Environmental Monitoring Center, Dalian 116023, China

Received 9 June 2015; accepted 3 December 2015

**Abstract:** In order to improve the discharge capacity and cyclic life of Mg–Co-based alloy, ternary  $Mg_{45}M_5Co_{50}$  (M=Pd, Zr) alloys were synthesized via mechanical alloying. TEM analysis demonstrates that these alloys all possess body-centered cubic (BCC) phase in nano-crystalline. Electrochemical experiments show that  $Mg_{45}Zr_5Co_{50}$  electrode exhibits the highest capacity (425 mA h/g) among the  $Mg_{45}M_5Co_{50}$  (M=Mg, Pd, Zr) alloys. And  $Mg_{45}Pd_5Co_{50}$  electrode lifts not only the initial discharge capacity (379 mA h/g), but also the discharge kinetics, e.g., exchange current density and hydrogen diffusion ability from that of  $Mg_{50}Co_{50}$ . It could be concluded that the electrochemical performances were enhanced by substituting Zr and Pd for Mg in Mg–Co-based alloy.

**Key words:** Mg-based electrode alloy; hydrogen storage; mechanical alloying; body-centered cubic structure; electrochemical performance; elemental substitution

### 1 Introduction

Mg-based hydrogen storage materials have attracted much attention during last decades due to their high capacity, relatively low cost and light mass [1,2]. They are also potential candidates for the anode materials of Ni–MH battery [3,4]. Series of Mg-based alloys, including Mg–Co-based alloys, have been developed in order to improve their properties in either gas–solid or electrochemical reaction systems [5–11].

Previous studies on Mg–Co alloys were mainly focused on their gaseous hydrogen storage performances. JEAN-LOUIS et al [12–14] achieved  $Mg_2Co$  alloy with face-centered cubic or amorphous phase, which absorbed maximum 4.5 atom hydrogen per formula unit to form  $MgH_2$  and  $Mg_2CoH_5$  (at 450 °C and 5 MPa for at least 1 h). Being inspired by Ti–V-based Laves related BCC alloy, the concept of Mg-based BCC alloy was first suggested about 10 years ago [15,16]. Their synthesized Mg–Tm–V (Tm=Ni, Co, Cu) alloys containing nano-

crystalline grains with BCC structure. Under the conditions of 298 K and 3 MPa ( $H_2$ ), their hydrogenation capacities attained 2.3%, 1.44% and 0.95%, respectively. After that, the Mg–Co-based BCC alloys were synthesized and investigated [8,9,17–19]. It was found that the single BCC structure can be obtained only within the Co mole fraction range of 37% to 80%. SHAO et al [17] revealed that the Mg–Co-based BCC alloy with lattice parameter of 0.3068 nm could achieve an optimized hydrogenation performance.

In our recent work, Mg–Co BCC alloys were initially introduced into anode material of Ni–MH battery system. Pd-doped  $Mg_2Co$  BCC alloy exhibits large discharge capacity of 530 mA h/g [10]. Co partially substituted by Pd in  $Mg_{50}Co_{50}$  can improve both initial capacity and cycling stability [11]. In this work, we paid more attention to the  $Mg_{45}M_5Co_{50}$  ternary alloys where Mg was partially substituted by Pd and Zr according to the enhancement of these elements in Mg-based alloy [10,11,20,21]. Their structures and electrochemical performances were intensively studied. Some

**Foundation item:** Projects (51471087, 61370042, 21173041, 11204031, 11472080) supported by the National Natural Science Foundation of China; Project (13KJA430003) supported by the Jiangsu Higher Education Institutions of China; Project (BK20141336) supported by the Natural Science Foundation of Jiangsu Province, China

**Corresponding author:** Yao ZHANG; Tel: +86-25-52091092; E-mail: zhangyao@seu.edu.cn

DOI: 10.1016/S1003-6326(16)64243-7

improvements in discharge capacities and cyclic stabilities were obtained.

## 2 Experimental

### 2.1 Material synthesis

The metal powders of Mg (99.99%, 75  $\mu\text{m}$ ), Co (99.99%, 10  $\mu\text{m}$ ), Pd (99.99%, 75  $\mu\text{m}$ ) and Zr (99.5%, 3  $\mu\text{m}$ ) were directly used without further treatment.  $\text{Mg}_{45}\text{M}_5\text{Co}_{50}$  (M= Pd, Zr) alloys were synthesized by ball milling the mixtures of these powders. 2 g sample and stainless steel (1Cr18Ni9Ti) balls with a diameter of 10 mm were loaded into each mill pot in a mass ratio of 1:30. All handles were operated in a Mikrouna Super 1220/750 glove box filled with argon with high purity (99.9999%,  $w(\text{H}_2\text{O}) < 0.1 \times 10^{-6}$ ,  $w(\text{O}_2) < 0.1 \times 10^{-6}$ ). The ball milling was conducted on a QM-1SP2 ball mill, lasting for 120 h at a rate of 450 r/min.

### 2.2 Material characterization

Scanning electron microscopy (SEM, FEI Sirion) was employed to observe the surface morphology of  $\text{Mg}_{45}\text{M}_5\text{Co}_{50}$  (M=Pd, Zr) alloys. Elemental distributions on surface of milled powder were identified by energy dispersive X-ray (EDS) analyses. Microstructures were investigated by transmission electron microscopy (TEM, FEI G2 20).

### 2.3 Electrochemical experiments

Each mixture of 100 mg sample powder with 400 mg nickel powders was pressed into a 10 mm-diameter tablet at 12 MPa and room temperature, which was sandwiched by foam nickel sheets and sealed by spot welding. The prepared anode would be measured on a three-electrode system where the counter electrode and the reference electrode were  $\text{Ni}(\text{OH})_2/\text{NiOOH}$  and  $\text{Hg}/\text{HgO}$ , respectively.

Charge–discharge tests were carried out on a CT2001A LAND battery measurement system. The charge and discharge densities were 100 and 30 mA/g, respectively. The cutoff potential was  $-0.6$  V (vs  $\text{Hg}/\text{HgO}$ ).

Electrodes at 50% depth of discharge (DOD) were adopted to test the linear polarization and alternating current impedance performances on an electrochemical workstation (CHI660C, Chenghua, Shanghai, China). The scanning range was from  $-5$  to  $5$  mV (vs open circuit potential) with a rate of  $1$  mV/s in linear polarization tests. Alternating current impedance measurements were operated at open circuit potential within the frequency range from  $10$  kHz to  $5$  mHz. Hydrogen diffusion activities were determined by potential step method with step difference of  $0.5$  V (vs open circuit potential) initially without DOD. To verify

the anti-corrosion properties of alloys, the Tafel tests were carried out before charging and after 100% DOD.

## 3 Results and discussion

### 3.1 Structures and morphologies of $\text{Mg}_{45}\text{M}_5\text{Co}_{50}$ (M=Zr, Pd) alloys

As we cannot obtain the precise microstructures and morphologies of the alloys merely through the XRD patterns [10,11,17–19], TEM images and the selected area electron diffraction (SAED) (shown in Figs. 1(a), (b) and Figs. 2(a), (b)) help to describe the morphologies of these alloys. The polycrystalline rings in TEM images for both samples were precisely investigated and summarized in Table 1. These radii's squares coincide well with Eq. (1), which demonstrates that  $\text{Mg}_{45}\text{M}_5\text{Co}_{50}$  (M=Zr, Pd) alloys contain single body-centered cubic (BCC) phase as that in  $\text{Mg}_{50}\text{Co}_{50}$  [11].

$$R_1^2 : R_2^2 : R_3^2 : R_4^2 : \dots = 1 : 2 : 3 : 4 : \dots \quad (1)$$

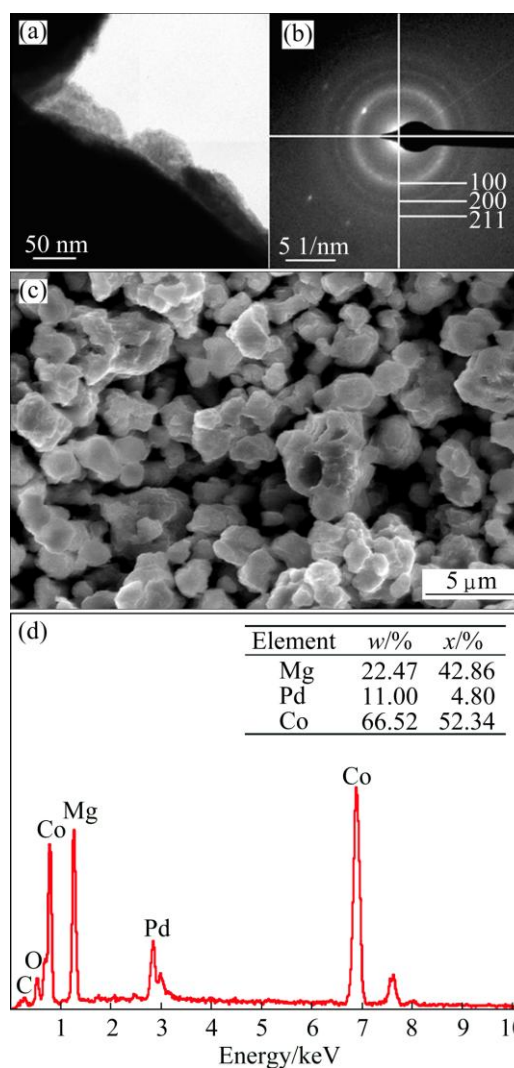


**Fig. 1** Morphology analyses of  $\text{Mg}_{45}\text{Pd}_5\text{Co}_{50}$  alloy: (a) TEM image; (b) SAED pattern; (c) SEM image; (d) EDAX result

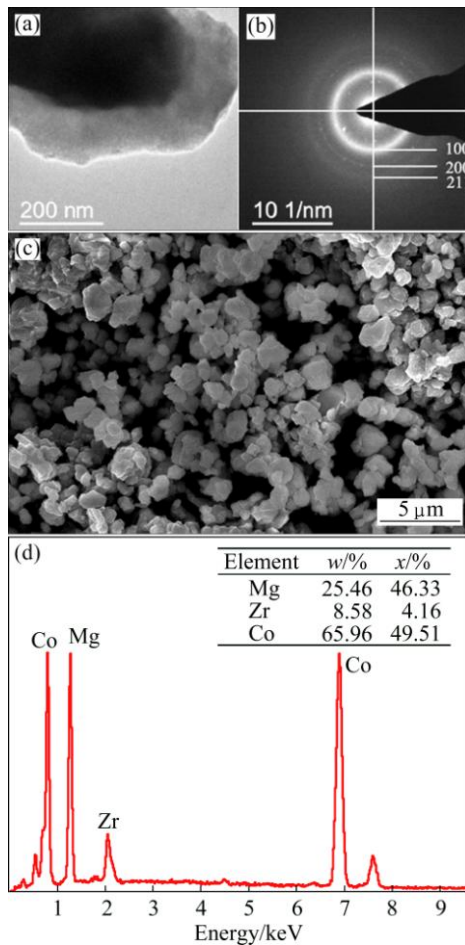


**Fig. 2** Morphology analyses of  $Mg_{45}Zr_5Co_{50}$  alloy: (a) TEM image; (b) SAED pattern; (c) SEM image; (d) EDAX result

By calculating the radii of rings, we obtained lattice parameters of 0.2969 and 0.2981 nm for  $Mg_{45}Pd_5Co_{50}$  and  $Mg_{45}Zr_5Co_{50}$ , respectively. Both are larger than that of  $Mg_{50}Co_{50}$  alloy (0.2946 nm) [11]. To the best of our

knowledge, the atomic radii of Pd and Zr are 0.179 and 0.216 nm, respectively. It is reasonable for these alloys that their lattice parameters increase with substituting these elements. The parameters' ascending order is as follows:

$$Mg_{50}Co_{50} < Mg_{45}Pd_5Co_{50} < Mg_{45}Zr_5Co_{50} \quad (2)$$

SEM analyses results (as shown in Figs. 1(c) and 2(c)) indicate that the sizes of particles range from 0.5 to 2  $\mu m$ . The elements of the alloy are all homogenously distributed on the surfaces of alloys according to EDS analyses (Figs. 1(d) and 2(d)).

### 3.2 Charge and discharge capability

Figure 3 shows the charge and discharge curves of the BCC electrodes in initial cycle.  $Mg_{45}Zr_5Co_{50}$  exhibit a plateau line at around  $-0.85$  V (vs Hg/HgO). No significant plateau can be observed in the discharge curve of  $Mg_{45}Pd_5Co_{50}$ , however, it still possesses a superior discharge capacity over binary  $Mg_{50}Co_{50}$ . According to our previous study [10,11], all alloys usually attain their maximum capacity at the first cycle. In this case, their initial capacities can be queued in ascending order as follows.

$$\begin{aligned} Mg_{50}Co_{50} (372 \text{ mA} \cdot \text{h/g}) < \\ Mg_{45}Pd_5Co_{50} (379 \text{ mA} \cdot \text{h/g}) < \\ Mg_{45}Zr_5Co_{50} (425 \text{ mA} \cdot \text{h/g}) \end{aligned} \quad (3)$$

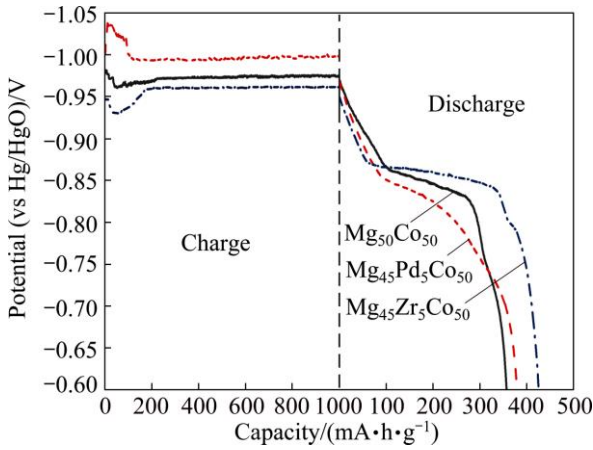
This order coincides well with that of Eq. (2), suggesting that the lattice parameters of the Mg–Co-based BCC alloys could be a factor in discharge capacity. One can find that the substitution of Zr for Mg in  $Mg_{50}Co_{50}$  possesses the highest discharge capacity.

Figure 4 reflects the dependence of the discharge capacities upon cycle number of the  $Mg_{45}M_5Co_{50}$  ( $M=$

**Table 1** Lattice parameters calculated by diffraction rings in SAED pattern of different alloys

Alloy	Ring No.	$r/\text{nm}^{-1}$	$r^2/\text{nm}^{-2}$	$r^2:r_1^2$	(hkl)	d/nm	a/nm
$Mg_{50}Co_{50}$ [11]	1	4.9610	24.6115	1.0000	(110)	0.2016	0.2851
	2	6.7517	45.5855	1.8522	(200)	0.1481	0.2962
	3	8.1214	65.9571	2.6799	(211)	0.1231	0.3016
	4	9.5658	91.5045	3.7180	(220)	0.1045	0.2957
Average lattice parameter/nm							0.2946
$Mg_{45}Pd_5Co_{50}$	1	4.7545	22.6053	1.0000	(110)	0.2103	0.2974
	2	6.7141	45.0791	1.9942	(200)	0.1489	0.2979
	3	8.2928	68.7705	3.0422	(211)	0.1206	0.2954
Average lattice parameter/nm							0.2969
$Mg_{45}Zr_5Co_{50}$	1	4.7268	22.3426	1.0000	(110)	0.2166	0.2992
	2	6.7432	45.4707	2.0352	(200)	0.1483	0.2966
	3	8.2021	67.2744	3.0110	(211)	0.1219	0.2986
Average lattice parameter/nm							0.2981

$r$ : Radius of diffraction ring; (hkl): Indices of crystal face;  $d$ : Interplanar distance;  $a$ : Lattice parameter



**Fig. 3** Initial charge and discharge curves of  $Mg_{45}M_5Co_{50}$  ( $M=Mg, Pd, Zr$ ) electrodes

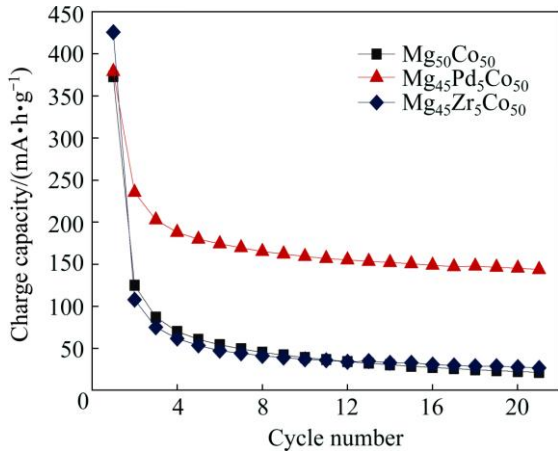


**Fig. 4** Discharge capacities of  $Mg_{45}M_5Co_{50}$  ( $M=Mg, Pd, Zr$ ) electrodes varied with cycle number

Mg, Pd, Zr). Their capacity retention rates at the 10th ( $C_{10}$ ) and the 20th ( $C_{20}$ ) cycles are summarized in Table 2. It is found that  $Mg_{45}Pd_5Co_{50}$  preserves around 40% of the maximum capacity at the 20th cycle. From the 10th cycle, the drastic decrease of capacity is slowed down. This indicates that Pd additive facilitates the enhancement of cycling stability, which agrees well with the previous observation on Pd-doped Mg–Ni alloy [4]. Furthermore, the cycling stability of  $Mg_{45}Pd_5Co_{50}$  electrode is more enhanced than our recently studied  $Mg_{50}Co_{45}Pd_5$  electrode shown in Table 2, suggesting that the substitution of Pd in Mg site is superior to that in Co

**Table 2** Initial discharge capacities ( $C_{max}$ ) and retention rates of  $Mg_{45}M_5Co_{50}$  ( $M=Mg, Pd, Zr$ ) and  $Mg_{50}Co_{45}Pd_5$  electrodes

$Mg_{45}M_5Co_{50}$	$C_{max}/(mA \cdot h \cdot g^{-1})$	$(C_{10}/C_{max})/\%$	$(C_{20}/C_{max})/\%$
$Mg_{50}Co_{50}$	372.77	10.49	6.04
$Mg_{45}Pd_5Co_{50}$	378.74	42.01	37.92
$Mg_{45}Zr_5Co_{50}$	425.49	8.70	6.28
$Mg_{50}Co_{45}Pd_5$ [8]	458.93	31.56	25.52

site in retaining the discharge capacities.

The high-rate discharge (HRD) ability ( $y$ ) can be characterized by Eq. (4) [22], where  $C_x$  stands for the capacity at discharge current density of  $x$  mA/g and  $C_{30}$  represents the residual capacity at current density of 30 mA/g.

$$y = \frac{C_x}{C_x + C_{30}} \times 100\% \quad (4)$$

Figure 5 shows that the  $y$  values of the electrodes generally decrease with the lift of discharge current density. With the introduction of Pd or Zr, the improvement in HRD ability can be easily observed from binary  $Mg_{50}Co_{50}$  electrode.

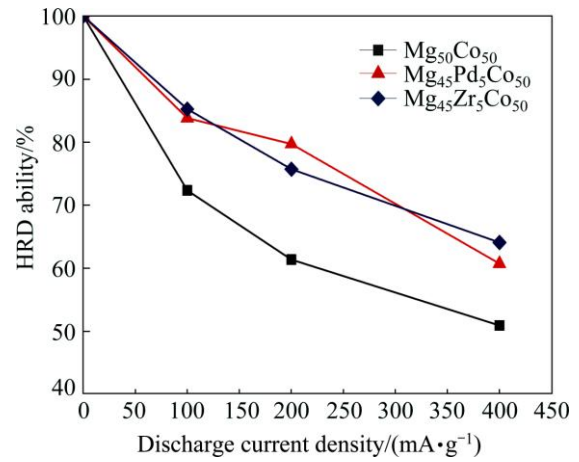


**Fig. 5** HRD ability curves of  $Mg_{45}M_5Co_{50}$  ( $M=Mg, Pd, Zr$ ) electrodes

### 3.3 Electrode reaction kinetics

#### 3.3.1 Linear polarization

In the present work, exchange current density ( $J_0$ ) and polarization resistance ( $R_p$ ) were employed for the purpose of describing the surface reaction kinetics of each electrode. According to the Butler–Volmer equation [23], the polarized current density  $J$  should depend linearly on the overpotential  $\eta$  as shown in Eq. (5), in which the overpotential was strictly limited in the linear polarization zone. Those scanning ranged from  $-5$  to  $5$  mV (vs open circuit potential).

$$J = \frac{J_0 F}{RT} \eta = \frac{\eta}{R_p} \quad (5)$$

where  $\eta$ ,  $J$ ,  $R$ ,  $T$  and  $F$  are overpotential, polarized current density, mole gas constant, temperature and Faraday constant, respectively.

Figure 6 displays  $J$ – $\eta$  curves of the electrodes obtained by linear polarization. Table 3 lists the  $R_p$  and  $J_0$  values determined by fitting curve. For additive Pd and Zr, the  $R_p$  resistances decrease with the increment of  $J_0$  over surface, and represent significant improvement in surface reaction rates from binary  $Mg_{50}Co_{50}$ .

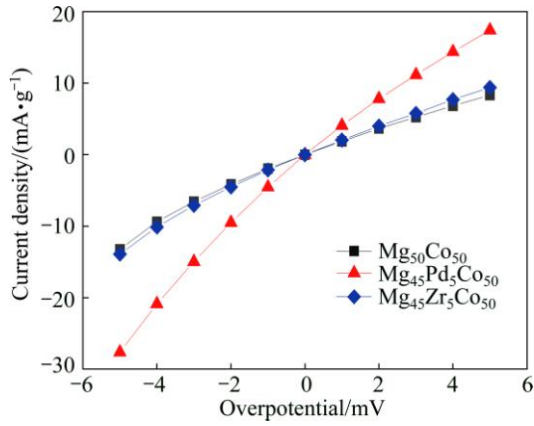


**Fig. 6** Linear polarization curves of  $Mg_{45}M_5Co_{50}$  (M=Mg, Pd, Zr) electrodes

**Table 3** Parameters of electrode reaction kinetics in  $Mg_{45}M_5Co_{50}$  (M=Mg, Pd, Zr) alloys

Alloy	$R_p/\Omega$	$J_0/(mA\ g^{-1})$	$R_{ct}/\Omega$	$D/(10^{-13}cm^2\ s^{-1})$
$Mg_{50}Co_{50}$	5.3576	50.05	5.54	0.68
$Mg_{45}Pd_5Co_{50}$	2.4549	109.03	0.88	1.10
$Mg_{45}Zr_5Co_{50}$	4.8195	55.08	4.28	1.07

3.3.2 Electrochemical impedance

Figure 7 shows the Nyquist plots of all the alloys being scanned in frequency from 10 kHz to 5 mHz. NOBUHIRO et al [24] suggested that there are normally four components including electrolyte resistance, two resistive components and a Warburg resistance component in equivalent circuit for metal hydride electrodes. In the present work, the absence of Warburg component in  $Mg_{50}Co_{50}$  and  $Mg_{45}Zr_5Co_{50}$  electrodes could be attributed to that the controlling step in the electrochemical reaction was charge transfer rather than diffusion over the surface. The semicircle in high-frequency range represents the contact impedance. The semicircle in middle-frequency range represents the charge-transfer process ( $R_{ct}$ ), which is relevant with  $R_p$  in surface reaction.  $R_{ct}$  in charge-transfer process was determined by fitting the Nyquist plot of each alloy. Table 3 exhibits that the variation of  $R_p$  corresponds well with the  $R_{ct}$  (also shown in Table 4). The  $R_{ct}$  of  $Mg_{45}Pd_5Co_{50}$  electrode is lower than that of  $Mg_{45}Zr_5Co_{50}$  and  $Mg_{50}Co_{50}$  electrodes, suggesting that the substitution of Pd plays a significant role in improving the electrode reaction kinetics.

**Table 4** Fitting results of Nyquist plots of  $Mg_{45}M_5Co_{50}$  (M=Mg, Pd, Zr) electrodes

Alloy	$R_s/\Omega$	$Q_1/(s^n \cdot \Omega^{-1})$	$n_1$	$R_1/\Omega$	$Q_2/(s^n \cdot \Omega^{-1})$	$n_2$	$R_2(R_{ct})/\Omega$	$Q_3(W_{1,R_3})/(s^n \cdot \Omega^{-1})$	$n_3(W_{1,Q_3})$	$R_{ct}(W_{1,n_3})/\Omega$
$Mg_{50}Co_{50}$	0.743	0.006	0.832	0.166	0.675	0.460	1.123	4.471	0.779	5.543
$Mg_{45}Pd_5Co_{50}$	0.592	0.017	0.714	0.146	0.365	0.607	0.883	0.0518	1.334	0.398
$Mg_{45}Zr_5Co_{50}$	0.563	0.035	0.755	0.109	0.965	0.498	8.189	4.388	0.789	4.278

$R_s$ : Solution resistance;  $Q$ : Impedance of CEP;  $n$ : Dispersion coefficient;  $W$ : Parameter in Warburg component

3.3.3 Hydrogen diffusion capability

Hydrogen diffusion coefficient is usually identified by the constant potential step according to Eq. (6) introduced by ZHENG et al [25].

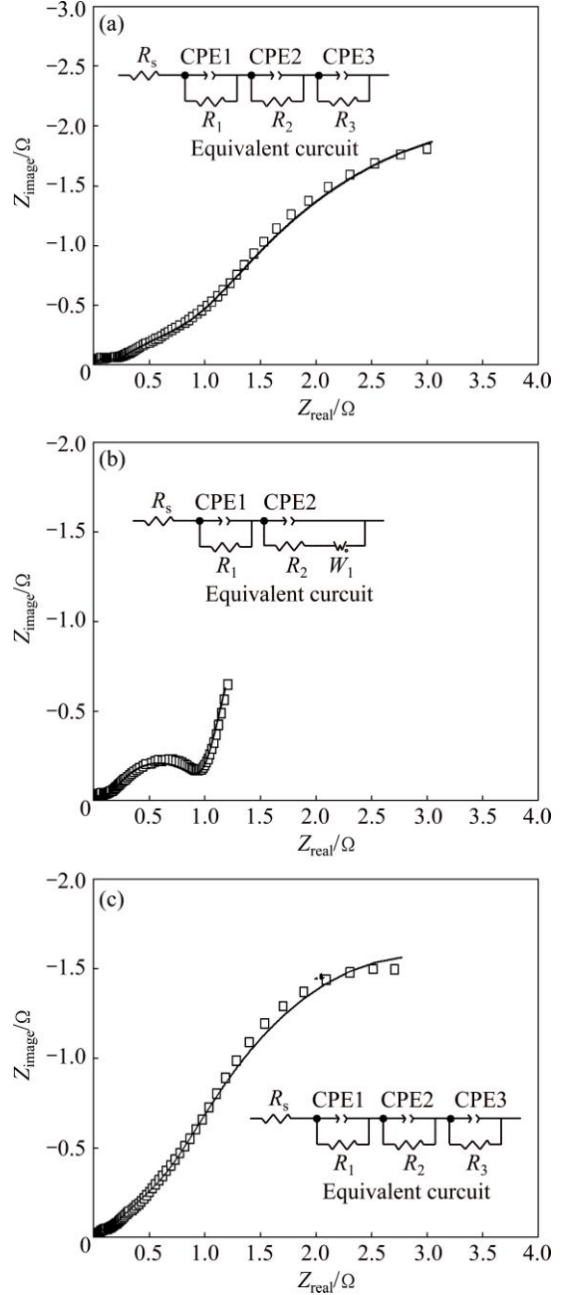


**Fig. 7** Electrochemical impedance spectra of  $Mg_{45}M_5Co_{50}$  (M=Mg, Pd, Zr) electrodes: (a)  $Mg_{50}Co_{50}$ ; (b)  $Mg_{45}Pd_5Co_{50}$ ; (c)  $Mg_{45}Zr_5Co_{50}$

$$\lg J = \lg \left[ \frac{6FD}{\rho a^2} (c_o - c_s) \right] - \frac{\pi^2 D}{2.303 a^2} t \quad (6)$$

where  $\rho$ ,  $a$ ,  $c_o$ ,  $c_s$ ,  $F$ ,  $D$  and  $t$  represent density of the alloy, sphere radius, constant bulk concentration, constant surface concentration, Faraday’s constant, diffusion coefficient and time, respectively. Equation (6) is derived when  $t$  is large.

Figure 8 presents plots of  $\lg J$  vs  $t$ , in which slopes ( $B$ ) of the linear parts in curves can be calculated by linear fitting. By virtue of Eqs. (6) and (7), the value of  $D$  is available to evaluate the hydrogen diffusion capability. The values of sphere radii were approximately 6  $\mu\text{m}$ , which was analyzed by SEM in Figs. 1 and 2.

$$D = \frac{2.303Ba^2}{\pi^2} \quad (7)$$

The achieved values of  $D$  are listed in Table 3. Compared with the binary alloy  $\text{Mg}_{50}\text{Co}_{50}$ , we found that the substitution of both Zr and Pd promotes the values of  $D$ , suggesting that the additives Zr and Pd are helpful for improving the hydrogen diffusion kinetics in alloys. This could be relevant with the higher HRD properties in  $\text{Mg}_{45}\text{Zr}_5\text{Co}_{50}$  and  $\text{Mg}_{45}\text{Pd}_5\text{Co}_{50}$  because the controlling step was hydrogen diffusion process of the alloy in high current density discharge.

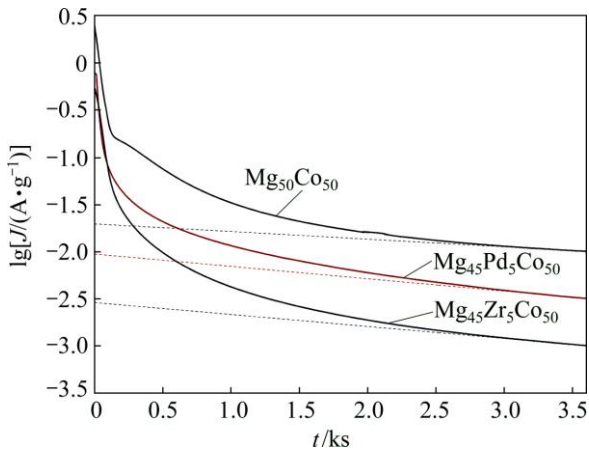


**Fig. 8**  $\lg J-t$  curves of  $\text{Mg}_{45}\text{M}_5\text{Co}_{50}$  ( $M=\text{Mg, Pd, Zr}$ ) electrodes obtained by potential step method

### 3.4 Corrosion performance

Tafel polarization curve could be available to describe the corrosion performance of alloys in alkaline electrolyte when the corrosion reaction dominates in electrochemical reaction. Tafel curves of alloys before charge and after initial discharge are demonstrated in Figs. 9(a) and (b), respectively, in which the electrodes became easier to be corroded after the first cycle. Meanwhile, the additive Pd or Zr shifts the corrosion potential  $\phi_{\text{corr}}$  to more positive direction. And the corrosion current densities (Fig. 9(c)) of alloys

determined by fitting Tafel curves also indicated that more enhanced corrosion-resistance abilities were achieved than that of binary alloy electrode. Therefore, the substitution of Pd exhibits the highest anti-corrosion ability in these alloys, which probably render the highest cycling stability of  $\text{Mg}_{45}\text{Pd}_5\text{Co}_{50}$ . This verifies again that Pd effectively inhibits the corrosion of the Mg–Co alloy in alkaline solution and improves the cyclic stability.

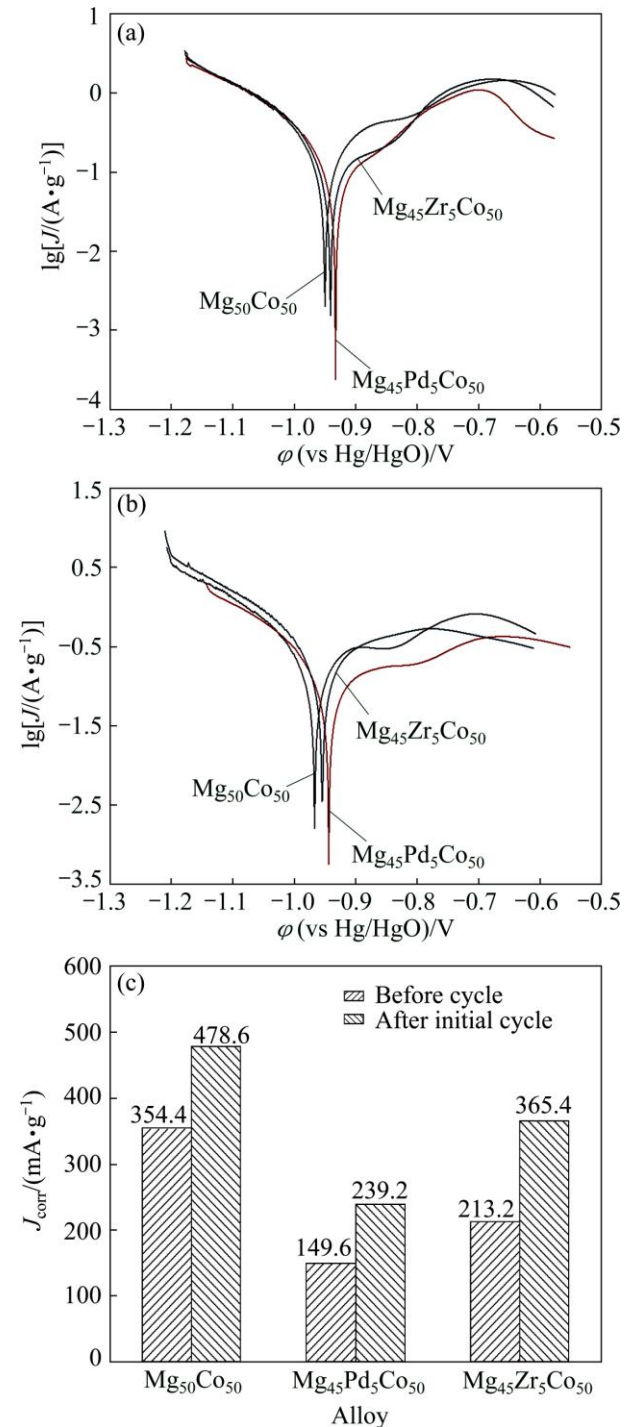


**Fig. 9** Tafel polarization curves of  $\text{Mg}_{45}\text{M}_5\text{Co}_{50}$  ( $M=\text{Mg, Pd, Zr}$ ) electrodes: (a) Before cycle; (b) After initial cycle; (c) Corrosion current density

## 4 Conclusions

1) XRD and TEM analyses exhibit that the major phase of  $Mg_{45}Pd_5Co_{50}$  and  $Mg_{45}Zr_5Co_{50}$  ternary alloys is BCC phase with lattice parameters of 0.2969 nm and 0.2981 nm, respectively.

2) The maximum discharge capacities strictly increase with the increase of lattice parameters for the Mg-Co-based BCC alloys. The  $Mg_{45}Zr_5Co_{50}$  electrode possesses the highest discharge capacity (425 mA h/g) as well as the largest lattice parameter.

3) The ternary  $Mg_{45}Pd_5Co_{50}$  alloy possesses the highest cyclic stability among the studied Mg-Co BCC electrodes.

4) In comparison with  $Mg_{50}Co_{50}$  and  $Mg_{45}Zr_5Co_{50}$  electrodes,  $Mg_{45}Pd_5Co_{50}$  electrode promotes not only the electrode reaction kinetics, but also the corrosion resistance and cyclic stability.

## References

- JAIN I P, LAL C, JAIN A. Hydrogen storage in Mg: A most promising material [J]. *International Journal of Hydrogen Energy*, 2010, 35: 5133–5144.
- DORNHEIM M, DOPPIU S, BARKHORDARIAN G, BOESENBERG U, KLASSEN T, GUTFLEISCH O, BORMANN R. Hydrogen storage in magnesium-based hydrides and hydride composites [J]. *Scripta Materialia*, 2007, 56: 841–846.
- ZHAO Xiang-yu, MA Li-qun. Recent progress in hydrogen storage alloys for nickel/metal hydride secondary batteries [J]. *International Journal of Hydrogen Energy*, 2009, 34: 4788–4796.
- YOUNG K, JEAN N. The current status of hydrogen storage alloy development for electrochemical applications [J]. *Materials*, 2013, 6: 4574–4608.
- SONG Wen-jie, LI Jin-shan, ZHANG Tie-bang, HOU Xiao-jiang, KOU Hong-chao, XUE Xiang-yi, HU Rui. Microstructure and hydrogenation kinetics of  $Mg_2Ni$ -based alloys with addition of Nd, Zn and Ti [J]. *Transactions of Nonferrous Metals Society of China*, 2013, 23(12): 3677–3684.
- KNOTEK V, VOJTĚCH D. Electrochemical hydriding performance of Mg-TM-Mm (TM=transition metals, Mm=mischmetal) alloys for hydrogen storage [J]. *Transactions of Nonferrous Metals Society of China*, 2013, 23(17): 2047–2059.
- ZHANG Yang-huan, XU Sheng, ZHAI Ting-ting, YANG Tai, YUAN Ze-ming, ZHAO Dong-liang. Hydrogen storage kinetics of nanocrystalline and amorphous Cu-Nd-added  $Mg_2Ni$ -type alloys [J]. *Transactions of Nonferrous Metals Society of China*, 2014, 24(11): 3524–3533.
- ZHANG Yao, YOSHINORI T, HIROTOSHI E, ETSUO A. The study on binary Mg-Co hydrogen storage alloys with BCC phase [J]. *Journal of Alloys and Compounds*, 2005, 393: 147–153.
- ZHANG Y, YOSHINORI T, HIROTOSHI E, ETSUO A. The hydrogen absorption-desorption performances of Mg-Co-X ternary alloys with BCC structure [J]. *Journal of Alloys and Compounds*, 2005, 393: 185–193.
- ZHANG Yao, ZHUANG Xiang-yang, ZHU Yun-feng, ZHAN Le-yu, PU Zheng-gan, WAN Neng, LI Li-quan. Effects of additive Pd on the structures and electrochemical hydrogen storage properties of  $Mg_{67}Co_{33}$ -based composites or alloys with BCC phase [J]. *Journal of Alloys and Compounds*, 2015, 622: 580–586.
- ZHANG Yao, ZHAN Le-yu, ZHU Yun-feng, ZHUANG Xiang-yang, GUO Xin-li, CHEN Jian, WANG Zeng-mei, LI Li-quan, QU Yi. The reversible hydrogen storage performances of  $Mg_{50}Co_{50}$  and  $Mg_{50}Co_{45}Pd_5$  alloys with body-centered cubic phase in electrochemical system [J]. *International Journal of Hydrogen Energy*, 2015, 40: 3944–3952.
- JEAN-LOUIS B, STANISLAS P, BERNARD C, BERNARD D. Preparation of  $Mg_2Co$  alloy by mechanical alloying: Effects of the synthesis conditions on the hydrogenation characteristics [J]. *Journal of Materials Chemistry*, 1999, 9: 315–318.
- JEAN-LOUIS B, ETSUO A, BERNARD D. Effect of substitution of Fe and Ni for Co in the synthesis of  $Mg_2Co$  compound using the mechanical alloying method [J]. *Journal of Alloys and Compounds*, 2000, 297: 192–198.
- JEAN-LOUIS B, ETSUO A, BERNARD D. Study of Mg-M (M = Co, Ni and Fe) mixture elaborated by reactive mechanical alloying: Hydrogen sorption properties [J]. *International Journal of Hydrogen Energy*, 2001, 26: 493–501.
- ETSUO A, IBA H. Hydrogen absorption by Laves phase related BCC solid solution [J]. *Intermetallics*, 1998, 6: 461–470.
- KUJI T, NAKAYAMA S, HANZAWA N, TABIRA Y. Synthesis of nano-structured BCC Mg-Tm-V (Tm=Ni, Co, Cu) alloys and their hydrogen solubility [J]. *Journal of Alloys and Compounds*, 2003, 356: 456–460.
- SHAO H Y, KOHTA A, HIROTOSHI E, ETSUO A. Fabrication, hydrogen storage properties and mechanistic study of nanostructured  $Mg_{50}Co_{50}$  body-centered cubic alloy [J]. *Scripta Materialia*, 2009, 60: 818–821.
- SHAO H Y, JUNKO M, LI H W, ETSUO A, ANKUR J, TAKAYUKI I, YOSHITSUGU K. Phase and morphology evolution study of ball milled Mg-Co hydrogen storage alloys [J]. *International Journal of Hydrogen Energy*, 2013, 38: 7070–7076.
- SHAO H Y, KOHTA A, HIROTOSHI E, ETSUO A. Correlation study between hydrogen absorption property and lattice structure of Mg-based BCC alloys [J]. *International Journal of Hydrogen Energy*, 2009, 34: 2312–2318.
- MUSTAFA A. Improvement of the electrochemical hydrogen storage performance of  $Mg_2Ni$  by the partial replacements of Mg by Al, Ti and Zr [J]. *Journal of Alloys and Compounds*, 2009, 486: 109–114.
- ZHUANG Xiang-yang, ZHANG Yao, ZHU Yun-feng, QU Yi, ZHAN Le-yu, WAN Neng, CHENG Hong-hui, GUO Xin-li, CHEN Jian, WANG Zeng-mei. The effects of Pd and/or Zr additives on the structures and cyclic stabilities of  $Mg_{50}Ni_{50}$ -based electrode alloys [J]. *International Journal of Hydrogen Energy*, 2015, 40: 2768–2774.
- STEEVE R, DANIEL G, LIONEL R. Comparative study on the structure and electrochemical hydriding properties of MgTi,  $Mg_{0.5}Ni_{0.5}Ti$  and  $MgTi_{0.5}Ni_{0.5}$  alloys prepared by high energy ball milling [J]. *Journal of Power Sources*, 2011, 196: 1561–1568.
- ALLEN J B, LARRY R F. *Electrochemical methods fundamentals and applications* [M]. 2nd ed. New York: John Wiley & Sons, 2001: 87–136.
- NOBUHIRO K, TETSUO S, HIROSHI M, ITSUKI U, HIROSHI I. Electrochemical impedance and deterioration behavior of metal hydride electrodes [J]. *Journal of Alloys and Compounds*, 1993, 202: 183–197.
- ZHENG G, BRANKO N P, RALPH E W. Electrochemical determination of the diffusion coefficient of hydrogen through an  $LaNi_{4.25}Al_{0.75}$  electrode in alkaline aqueous solution [J]. *Journal of the Electrochemical Society*, 1995, 142: 2695–2698.

## $Mg_{45}M_5Co_{50}$ (M=Pd, Zr)三元贮氢电极的电化学性能

詹乐宇<sup>1</sup>, 张耀<sup>1</sup>, 朱云峰<sup>2</sup>, 庄向阳<sup>1</sup>, 万能<sup>3</sup>,  
曲翊<sup>4</sup>, 郭新立<sup>1</sup>, 陈坚<sup>1</sup>, 王增梅<sup>1</sup>, 李李泉<sup>2</sup>

1. 东南大学 材料科学与工程学院, 南京 211189;
2. 南京工业大学 材料科学与工程学院, 南京 210009;
3. 东南大学 电子科学与工程学院, 南京 210096;
4. 大连市环境监测中心, 大连 116023

**摘要:** 为了提高 Mg-Co 系合金的放电容量及循环稳定性, 通过机械合金化的方法, 制备三元  $Mg_{45}M_5Co_{50}$  (M=Pd, Zr) 合金。透射电子显微镜(TEM)分析表明, 合金为体心立方相(BCC)的纳米晶结构。电化学测试表明, 在  $Mg_{45}M_5Co_{50}$  (M=Mg, Pd, Zr)合金中,  $Mg_{45}Zr_5Co_{50}$  电极的容量最高, 达到 425 mA h/g; 相比  $Mg_{50}Co_{50}$ ,  $Mg_{45}Pd_5Co_{50}$  电极的首次放电容量(379 mA h/g)与电化学动力学性能均得到提高。结果表明, 通过用 Zr 和 Pd 元素替代 Mg 元素, Mg-Co 基合金的电化学性能得到改善。

**关键词:** Mg 基电极合金; 贮氢; 机械合金化; 体心立方结构; 电化学性能; 元素替代

(Edited by Wei-ping CHEN)